Graphene-based Interconnects for Stable Dye-Sensitized Solar Modules

Paolo Mariani[1], Antonio Agresti[1], Luigi Vesce[1], Sara Pescetelli[1], Alessandro Lorenzo Palma[1,2], Flavia Tomarchio[3], Panagiotis Karagiannidis[3], Andrea C. Ferrari[3,] and Aldo Di Carlo,[1,4,5,*]*

[1]CHOSE- Centre for Hybrid and Organic Solar Energy, Department of Electronics Engineering, University of Rome "Tor Vergata", via del Politecnico 1 00133 Rome – ITALY

[2]Italian National Agency for New Technologies, Energy and Sustainable Economic Development (ENEA), Energy Efficiency Unit Department, Via Anguillarese, 301, 00123 Santa Maria di Galeria (Rome), Italy

[3]Cambridge Graphene Centre, University of Cambridge, 9 JJ Thomson Avenue, Cambridge CB3 0FA, UK

[4]Istituto di Struttura della Materia, National Research Council (CNR-ISM), Rome (Italy)

[5]LASE – Laboratory for Advanced Solar Energy, National University of Science and Technology – MISIS, Moscow (Russia)

Corresponding authors: aldo.dicarlo@uniroma2.it; acf26@eng.cam.ac.uk

ABSTRACT

We present Z-Type Dye Sensitized Solar Modules (DSSMs) with screen printed graphene-based vertical interconnects. This module architecture allows us to prevent corrosion of graphene interconnects once in contact with electrolytic species, unlike conventional Ag interconnects. By enlarging the width of single cells, or by increasing the number of cells, we get an enhancement of the aperture PCE of +12% with

respect to Ag-based modules, with 1000h stability under 85 °C stress test. This paves the way to original design layouts with decreased dead area and increased generated power per aperture area.

Keywords: Graphene, Dye Sensitized Solar Modules, Vertical Contact, Large Area Deposition, Stability

1. INTRODUCTION

The installation rate of photovoltaic (PV) technologies has increased by two orders of magnitude over the last 15 years,[1] from ~1 (GW)/year in 2004,[2] to ~100 GW/year in 2018.[2] This growth fostered the development of new PV technologies that better suit specific applications with respect to conventional Si cells. Dye Sensitized Solar Cells (DSSCs)[3, 4] are photo-electrochemical cells[5], ideal for Building Integrated Photo-Voltaic (BIPV)[6-8] and for energy harvesting in indoor-light condition.[9] DSSC have better response to diffuse light compared to traditional semiconductor PV technology[10], due to the mesoporous structure of the cell allowing omnidirectional light harvesting,[11] an almost constant Power Conversion Efficiency, PCE, i.e. the ratio between incident solar photon energy on the cell and electrical energy output,[12] as a function of inclination angle[13] (i.e the angle of the PV plane with the horizontal)[14], and can have transparency>50%[15, 16] and show one of the highest (>60%) transmission rate percentage of the solar radiation through the PV unit,[17] among TPVs (Transparent Photovoltaics) technologies.

Typically, DSSC technology is based on cells made of two conductive transparent glass substrates:[18] 1) Photo-electrode (PE) coated with mesoporous TiO_2. 2) Counter-electrode (CE) coated with Pt clusters,[19] or carbon-based materials.[20] Dye molecules are adsorbed on TiO_2 by immersing the PE into a dye solution.[21, 22] The electrons of these molecules, excited by light, are injected in the conduction band of TiO_2[23, 24] and subsequently transferred to Fluorine doped Tin Oxide (FTO), the most common Transparent Conductive Oxide (TCO) covering the glass substrates for DSSCs.[10] Oxidized dyes can recover electrons via a redox reaction with the electrolytes (typically iodide/triiodide, I^-/I_3^-) inserted into the cell.[23, 25, 26] The

reduction of the electrolyte occurs at the CE, catalysed by the Pt. DSSCs are scalable to large (>10cm^2) area by employing sheet-to-sheet printing.[27] By scaling DSSCs to large area modules (from 100 to 1000 cm^2),[27] a reduction of PCE is observed,[28] due to the impact of substrate resistivity. This is counteracted by printing conducting grids[29] or by making cells of smaller dimensions connected in various ways[30]. The cells of a Dye-Sensitized Solar Module (DSSM) can be either connected in parallel (currents of the cells are summed) or series (voltages of the cells are summed), with 4 possible module architectures: i) parallel,[29, 31, 32] ii) series monolithic,[33, 34] iii) series W-type (where the polarity of adjacent cell is inverted)[35, 36] and iv) series Z-type (where adjacent cells have all the same polarity).[37-39] In the latter configuration, the module is composed by identical cells sandwiched between two scribed conducting glass plates, with conducting vertical connections (typically Ag) connecting adjacent cells.[40-42]

A Z connection guarantees uniform and reliable output over large areas in different illumination and temperature (T) conditions, such as orientation with respect to the Sun[43] and a T range= -40°-85°C,[37] and achieves the best PCE among the different DSSMs architectures.[40, 44] The Active Area (AA) of a module[45] is dedicated to the solar energy conversion, while the dead area (DA)[40, 45] is needed for the interconnects and their protection. The aperture ratio is defined as AR = AA/(AA+DA), where the sum of AA and DA is the aperture area (APA).[40, 45] One of the major drawbacks of DSSMs is the electrolyte corrosive action on the metal grids.[46, 47] Thus, a rugged encapsulation is needed to isolate the electrolyte chamber from metal connections and to mechanically keep firm the two electrodes.[48] This safety area surrounding the Ag grids is greater than the surface occupied by the same Ag grids. However, this layout unavoidably reduces AR.

Ref.39 first reported a Z-type DSSM and connected 64 DSSMs (100 cm^2) in series to form a large panel. They performed an outdoor stability test comparing, over 6 months, the DSSMs electric power with a crystalline Si module of similar electric power rating. The major issue during fabrication was the DSSM sealing, which resulted in performance degradation.[48] This was overcome by Refs.37, 49, where glass frit was used as sealant, processed at T>600 °C in atmosphere, giving a PCE~3.5 % on~30 cm^2, showing a low

(<55%) Fill Factor, FF, i.e the ratio of cell maximum power output to the product of its open-circuit voltage V_{OC} and its short-circuit current I_{sc},[50] and low (<0.5 mA/cm^2) short circuit density current (J_{SC}).[48] 100cm^2 modules were reported[51] with a PCE~6.3%. In Ref.[51] a significant enhancement in FF and J_{SC} was achieved by decreasing the width of each individual strip (~0.8 cm). FF and J_{SC} depend on the width of each TiO_2 cell and much less on their lengths.[41, 52] Following this approach, Ref.40 realised a DSSM using a reflective/diffusive CE, with~6.9% PCE on APA~43 cm^2, and~9.4 % on AA~31 cm^2, by using a multilayer TiO_2 in combination with $TiCl_4$ treatment.[53] As of July 2020, the certified record, but without information on stability, is~8.8 ± 0.3% on 400 cm^2 (26 cells in series) and ~10.7 ± 0.3% on 26 cm^2 (7 cells in series, mini-module).[44]

Z-type modules have 3 main problems[48]: i) liquid electrolytes corrode Ag-based electrical contacts (which reduces the options for scale up of DSSCs to module size),[54] ii) AA is reduced with respect to APA, due to the need of additional sealing to protect the vertical connections, i.e. 3 layers of seal/conductor/seal for each interconnect,[36, 55] iii) the fabrication process is more complex (more steps) with respect to other configurations, such as W (not requiring connection grid).[36, 56]

Vertical connections can create difficulties when assembling the electrodes, since tolerances in variations in height of the vertical connections and sealants are tight (~5µm).[28] Corrosion of Ag connections significantly affects stability.[57] Thus, interconnects need to be protected from electrolyte corrosion via sealing. In DSSMs, sealant is also used to prevent electrolyte leakage,[26] evaporation of solvents,[58] delamination of substrates,[59, 60] electrolyte bleaching[61] and to fix the distance (i.e. chamber) between the electrodes (typically~20-60 µm).[55, 59, 62, 63] The most common sealants are thermoplastics, such as Surlyn,[64, 65] Bynel[55, 64, 66, 67] or glass frit.[68] Ref.[65] reported that very large area (10 modules of 15 cm^2, arranged in a panel) device assembled with glass frit retained~86% of the initial PCE, after an outdoor test of 47 days in summer. Ref.65 also showed that glass frit sealed small area cells (<0.2 cm^2) lost only~2.3% of the initial PCE compared to~34% of Surlyn. However, glass frit requires an immersion of PE

in the dye solution after assembling the device, because the dye would be destroyed at the T needed to process the glass frit (~600°C).[37, 49] Very low PCEs (<2%) were reported for large area (23 cm^2) devices[69] with glass frit, without using any Ag grid. To the best of our knowledge, accelerated and outdoor tests on sealants for Z-type DSSMs are lacking, hampering the industrialization of this technology.[46]

The interconnection strategy to obtain efficient and stable Z-type modules, according to ISOS (International Summit on Organic Photovoltaics Stability) tests[70] based on IEC (International Electrotechnical Commission) International Standards[71] is still an open technological issue. Ref.[72] replaced Ag interconnects with a Ti-based compound (~45µm Ti particles and 5µm W particles in a polymer matrix) less sensitive to electrolyte corrosion. Although the resulting vertical connections are less conductive than Ag, implying a reduction of module PCE (due to a FF reduction), a new design without additional sealing for interconnections could be used. Ref.[73] applied a layer of non-metallic material, such as TiN, ZrN, boron carbide, to protect the metallic (e.g. stainless steel) conductors from the electrolytic species (e.g triiodide/iodide). These non-metallic materials are chemically inert to the conductors, which act as vertical connection. This introduces an additional complexity to manufacture the non-metallic grids, leading to loss of module bifaciality, i.e the possibility to be illuminated from both sides.[74, 75]

Graphene and related materials (GRMs) can be used in several solar cell technologies[76, 77] such as Si,[78, 79] polymer/organic[80, 81] and Perovskite (PSC).[82, 83] In PSC, few-layer graphene (FLG) was combined with mesoporous TiO_2,[84-86] lithium neutralized graphene oxide (GO-Li) was employed as interlayer at $mTiO_2$/perovskite interface,[87] while GO was used as a hole transport material (HTM) to replace standard spiro-OMeTAD.[88] GRMs have been incorporated into DSSCs with a variety of roles.[89, 90] Ref.[91] reviewed the use of graphene-based composites as CE in DSSCs replacing or in combination with Pt. This strategy was demonstrated on small area cells (~0.38cm^2) showing a lower charge-transfer resistance, R_{CT}, of the CE based on graphene-flakes used in combination with ionic liquid electrolyte, when compared to traditional electrolytes in methoxypropionitrile (MPN).[92] A CE prepared from a graphene ink was used on large area

modules achieving~3.5% PCE on~43.2 cm^2 AA.[66] Ref.[93] combined stable aqueous dispersion of graphene flakes, prepared by non-covalent functionalization with 1-pyrenebutyrate (PB^-), with PEDOT-PSS as catalyst in small area~0.072 cm^2 cells, achieving PCE~4.5%. Ref.[94] incorporated GO, obtained by a modification of the procedure of Ref.[95] in the TiO_2 film to obtain higher light harvesting in the visible region. A typical DSSC has a~6−15 µm thick layer of TiO_2[96] and electrons photo-generated in the inner part of the photo-electrode have to percolate through TiO_2 particles and be collected at the photo-electrode (~100µm length assuming a random walk).[97] Ref.[98] proposed the use of GO as an electron bridge in the photo-anode, shuttling electrons to the current collector and lowering recombination. In Ref.[98], GO was found to induce macropores in the TiO_2 films, acting as scattering centres and improving J_{SC} and PCE. Poly-crystalline FLG deposited by Chemical Vapour Deposition (CVD), covering homogeneously~1cm^2, was used to replace the transparent conductive film (TCF).[99] FLG nanoribbons, produced by catalytic CVD on Si, either attached to the CE, or dispersed into the electrolyte, induced optical transparency of an iodide/triiodide redox couple in a DSSC, resulting in a ~22% increase in PCE, when measured from the CE side.[100] In Ref.[101], the TiO_2 surface was modified with ~2nm Graphene Quantum Dots (GQDs) in order to promote light absorption, enhancing J_{SC}~30% and PCE~27% with respect to cells with pristine TiO_2.

Here we use graphene-based screen-printed vertical interconnects in Z-type DSSMs as alternative to the common Ag paste. The superior stability and PCE on APA of our graphene-based interconnects against electrolyte-induced degradation is demonstrated by removing the sealing and increasing AA~25%. The resulting modules show an improvement in PCE on APA up to 12% with respect to Ag-based ones. We also show that graphene can be used in DSSMs to overcome grid corrosion. Our work can be applied to any combination of active materials within Z-type modules, such as TiO_2, Pt (or any carbon-based CE), dye and electrolyte, already shown to improve J_{SC}, V_{OC} and FF.

2. RESULTS AND DISCUSSION

Graphene is prepared by microfluidization of graphite (Timrex KS25) in water and sodium deoxycholate (SDC).[102] Microfluidization applies high pressure (up to~207MPa)[103] to a fluid, forcing it to pass through a microchannel (diameter<100μm).[102, 103] The key advantage over sonication[104, 105] and shear-mixing[106] is that a high shear rate > 10^6 s^{-1} is applied to the whole fluid volume[107] not just locally, resulting in a uniform processing and no material wastage.[102] The lateral size of the exfoliated flakes dispersed in deionized (DI) water (graphene-ink concentration is~9 g/L) is~1μm.[102] A representative Raman spectrum of the processed flakes after 70 cycles is shown in Fig.1, acquired at 514 nm. The 2D band lineshape shows two components ($2D_2$, $2D_1$). Their intensity ratio $I(2D_2)/I(2D_1)$ changes from~1.5 for starting graphite to~1.2 for 70 cycles indicating exfoliation, but not complete to single layer.[102, 108]

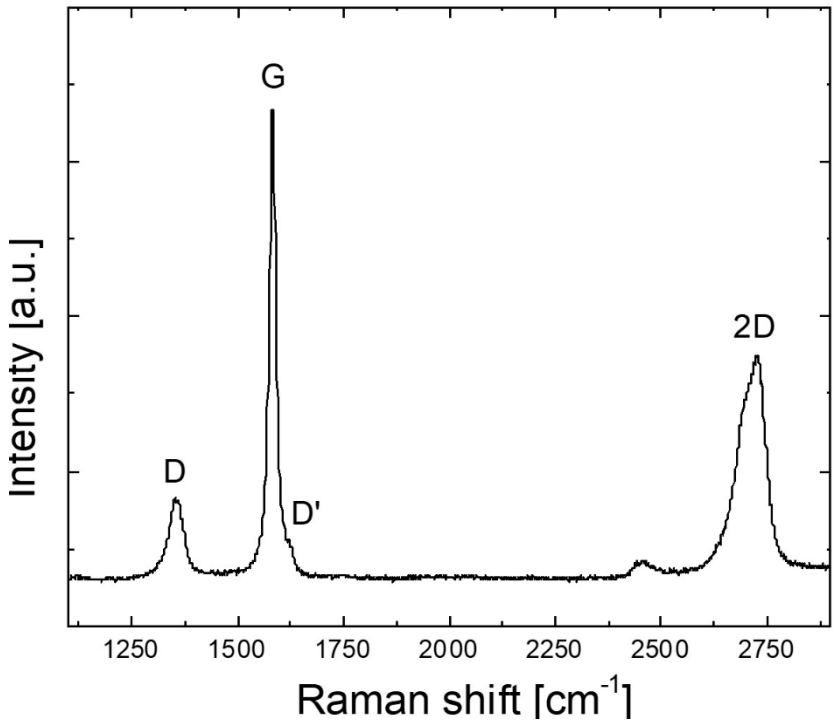

Fig. 1: Representative Raman spectrum at 514.5 nm for microfluidized flakes after 70 cycles.

The DSSMs are then prepared as follows.

First, we describe the fabrication process for standard devices with Ag vertical interconnects.

Two 2.2 mm-thick FTO/glass substrates are cut and prepared to act as PE (65 or 60 mm in width) and CE (65 or 60 mm in width). The glasses are cleaned in an ultrasonic bath before with acetone, then with

ethanol and finally UV-O_3 treated to remove organic contaminations[109], as well as improve wettability.[110] The two glasses are then etched (Fig.2a) by means of a Nd:YVO_4, λ= 1064 nm raster scanning laser[45] in order to separate the cells within each substrate.[45] On both electrodes, Ag paste is screen-printed (Fig.2b) in order to realize the vertical contact. The thickness of this vertical contact is~20µm for each electrode. Then, we deposit onto the PE (Fig.2c1) by screen printing, two layers of TiO_2 paste based on 20nm TiO_2 particles. The first layer is dried at 120°C for 20 min before printing the second one.

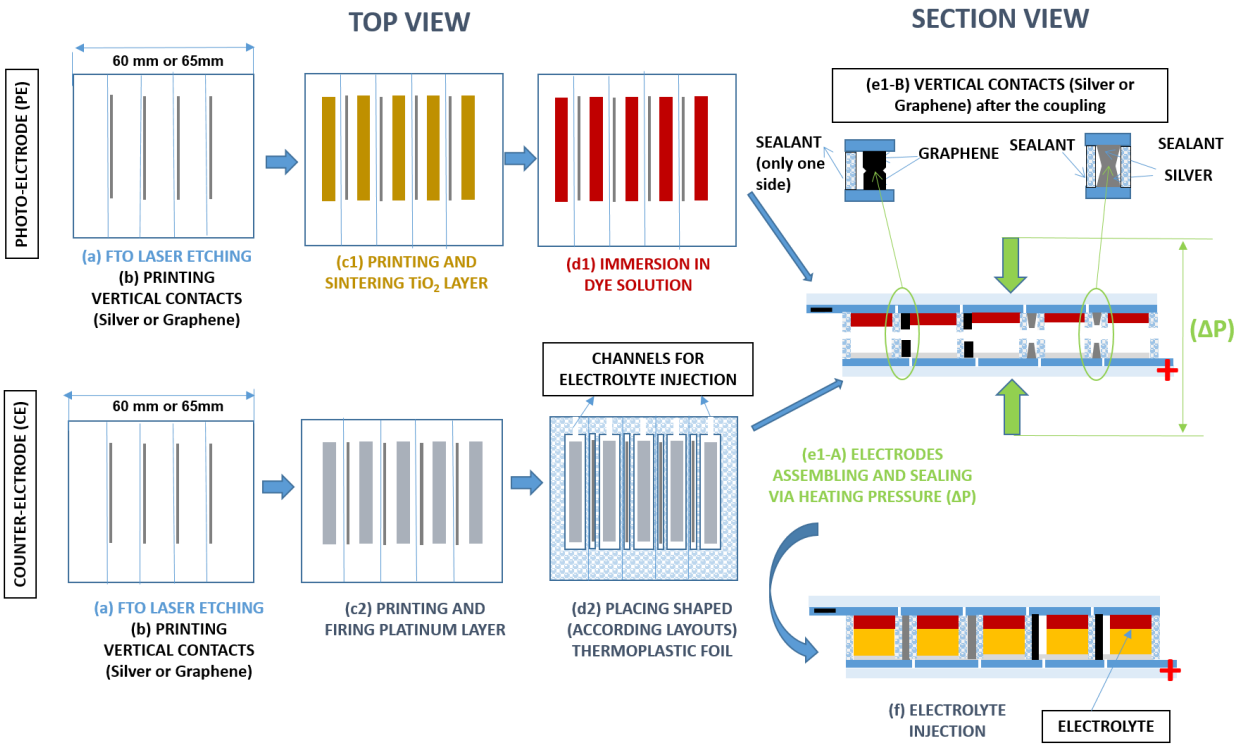

Fig. 2: fabrication process of a Dye Sensitized Solar Module with vertical contacts (Z-Type). (a) laser etching of FTO (in simple blue) both on PE and CE, (b) deposition of vertical contacts, (c1) deposition and sintering of TiO_2 (in ochre yellow), (c2) deposition and firing of Pt (in grey), (d1) PE immersed in dye solution (in red), (d2) placing shaped thermoplastic foil (in textured blue) on CE, (e1-A) assembling and sealing PE and CE by mean of heat pneumatic press, (e1-B) zoom of vertical interconnects for graphene and and Ag-based modules, (f) electrolyte (in yellow) injection by vacuum back filling.

The PE is then sintered at 480°C for 30min to decompose the organic binders in the paste and to promote electromechanical bonding between the TiO_2 NPs.[111] The final thickness is~11-12 µm, as measured via profilometry. This is the optimum value to obtain the best PCE and J_{SC} for a DSSC device.[112, 113] On the CE

(Fig.2(c2)) a double layer of Pt is screen-printed. The first is dried at 120° C for 10 min before printing the second one. Then, the CE is fired at 480°C for 30 minutes, i.e. baked in an oven to assure the complete volatilization (i.e. conversion to CO_2) of all organic components, such as terpineol, of the Pt paste.[114 19] The PE is then immersed overnight (Fig.2(d1)) in a dye N719 solution in Ethanol (0.3 mM), in order to sensitize (i.e. put the PE in condition to react to light by the mediation of a light-absorbing molecule, i.e. the dye)[21, 24] the TiO_2 film, and then rinsed ethanol. We consider N719 as a benchmark dye. However, the stability of N719 upon a light soaking stress (at 1 SUN, 1000 hours) is limited, since it loses>30% of its initial PCE, while organic dyes maintain>88% of their initial efficiency.[115] N719 is also a Critical Raw Material (CRM) since it contains Ru.[116] Thus, we opt for the organic dye DN-F05 for stability analysis, even though both N719 and DN-F05 have similar efficiency in DSSMs. DN-F05 is not a CRM,[116] and allows us to get similar PCE to N719, increasing the sustainability and the greenness of the resulting devices. Then, the two electrodes are thermally (at 150°C) sealed (Fig.2(e)) with a thermoplastic foil already placed onto CE (Fig,2(d2)) and shaped to protect the grids, by the pressure applied with an automatic pneumatic heat press. An electrolyte is then injected (Fig.2 (f)) by vacuum back filling[117] through the channels, one for each cell, realized in the thermoplastic foil (Fig.2(d2)). These are subsequently sealed with a commercial acrylic resin or closed with the pneumatic heat press.

The fabrication process for the devices with graphene-based vertical contact is the same for the standard ones, except for the step (b) in Fig.2. In this case, we use the graphene-based ink in order to realize the vertical contact. Via screen printing, we deposit 6 superimposed layers that reach 25µm thickness on each of the two electrodes. Each layer is dried with N_2 for few seconds to ensure a better adhesion of the subsequent layer.

For TLM (Transfer Length Method)[118-120] measurements, we print six, equally dimensioned in width (W) and length (L) (Fig.3a), Ag (1 layer, as in the Ag-based devices) and graphene (six superimposed layers, as in the graphene-based devices) contacts on two FTO/glass substrates, at increasing distances (d_i), and

insulate single contact stripes by raster scanning a 15 ns Nd:YVO_4 laser at 1064 nm with a fluence 12 J/cm^2. The resistance R between different contacts is then measured and plotted as a function of d_i, in Fig.3b.

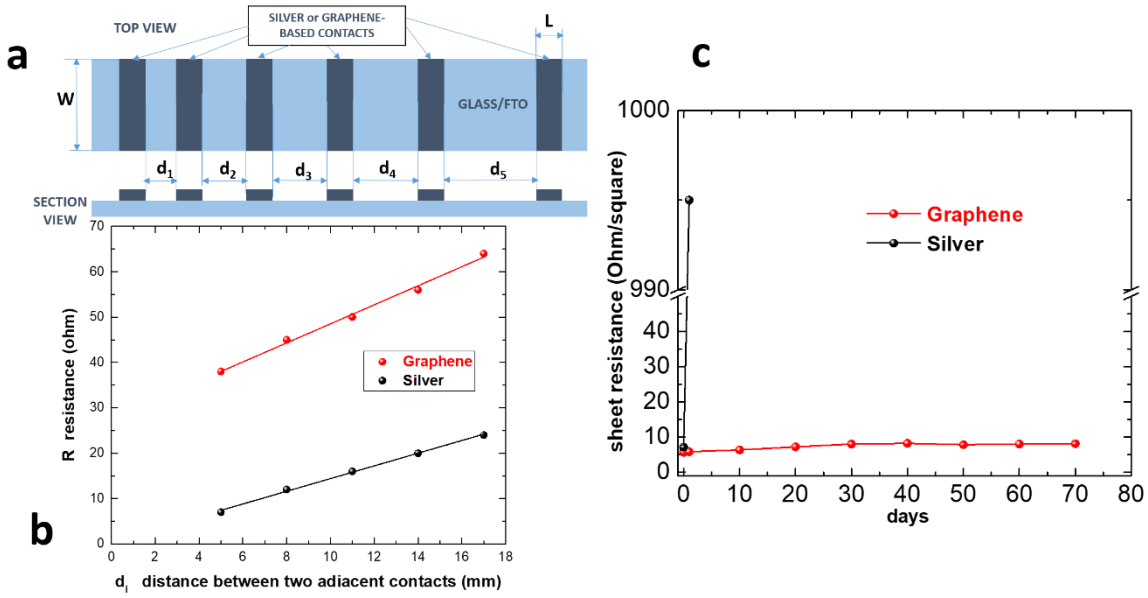

Fig3. a) TLM measurement setup. b) TLM experiments on Graphene and Ag contacts. c) R_S of screen-printed graphene and Ag immersed in HSE electrolyte over 10 weeks.

We derive the transfer length (L_T), i.e. the effective length over which the current that flows in a layer sitting under a metal contact is transferred into the latter, from:[119]

$$L_T = \sqrt{\frac{1}{R_{SH}\, G_C}} = \sqrt{\frac{\rho_C}{R_{SH}}} \qquad (1)$$

where R_{SH} is the sheet resistance of the layer sitting under the contact, G_C is the conductance of the contact between the metal and the underneath layer, and ρ_C the contact resistivity.

A test on electrolyte corrosion resistance of the graphene-based printed fingers is then carried out. A 5cm^2, 6µm thick, film is deposited and annealed on a non-conductive glass. The resulting sheet resistance, R_{SH}~5-9 Ω/sq is similar to FTO-covered glass (~7-8 Ω/sq). This is then immersed in HSE (High Stability Electrolyte). R_{SH} measurements are then carried out in 9 sites of the square sample surface. Fig.3c shows that, when starting from R_{SH}~5 Ω/sq, this reaches~7 Ω/sq after 20 days and remains almost constant along the following days (measurements done every 10 days).

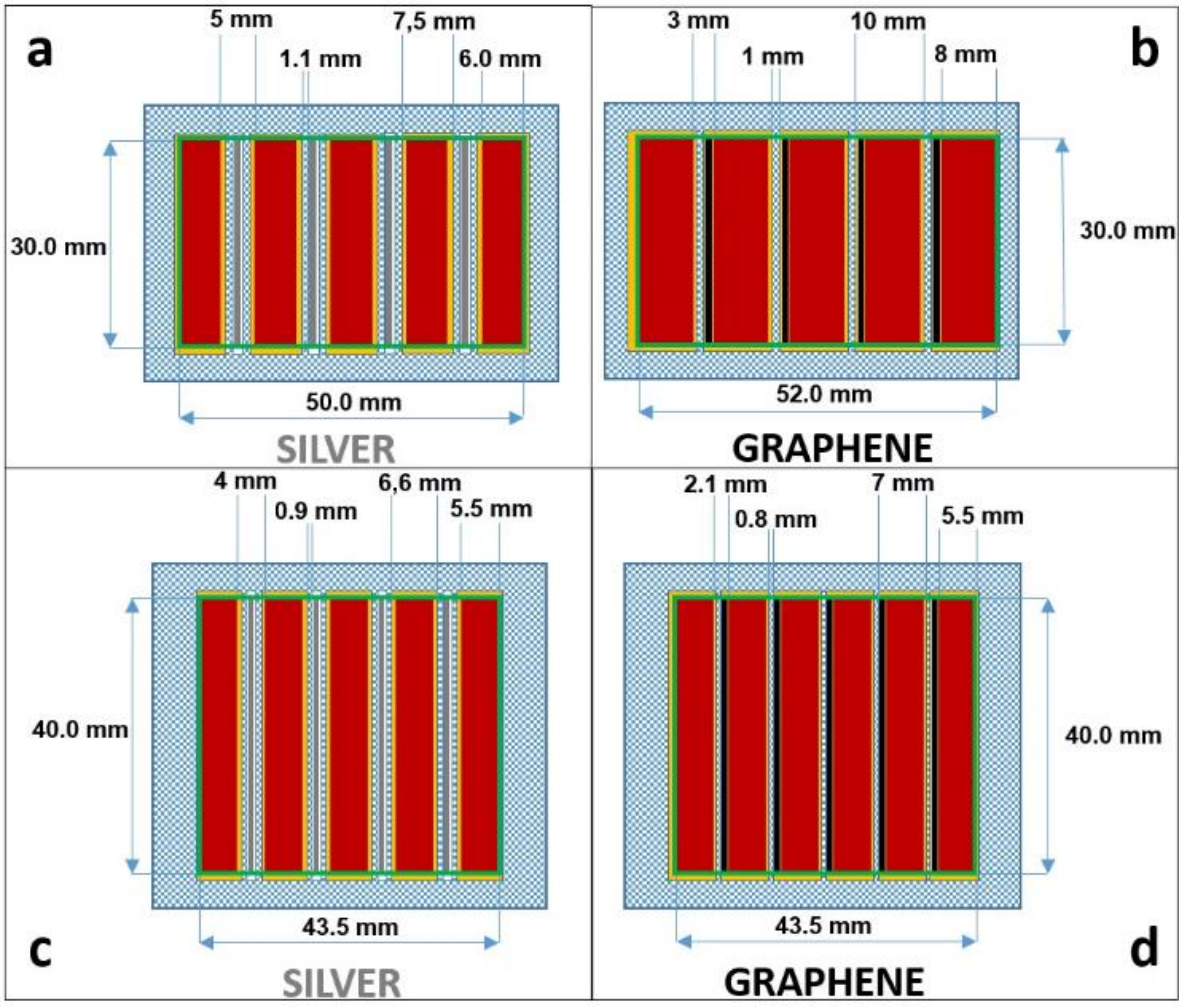

Fig 4: DSSMs layouts. a, b) modules (top view of the PE) with same number of cells, a) Ag-based, b) graphene-based. The reduction of the sealing area in graphene based DSSMs allows us to increase the cell width with respect to Ag (Layout A). c,d) two modules (top view of the PE) having c) 5 (Ag-based) and d) 6 cells (graphene-based). Due to the reduction of sealing area, a larger number of cells can be accommodated in the graphene-based module (Layout B). The grey lines in a,c) depict the Ag contacts, the black lines in b,d) depict the graphene-based contacts. In a-d) the sealant is shown as a textured blue grid, the AA (TiO_2+dye) is in red, the electrolyte in yellow, the surface corresponding to APA is shown by green boxes.

After 70 days, R_{SH} is still~8 Ω/sq. For the Ag film, after 1 day Ag sheets are seen floating in the electrolyte, and R_{SH} goes from~7 Ω/sq to~1 kΩ/sq. This shows that the graphene-based ink is less affected by electrolyte than Ag, paving the way to the fabrication of devices in which the contact between electrolyte and interconnects is allowed. Refs.[94, 121] showed that the dye can attach onto graphene. However, in our

case this is not responsible for the chemical sturdiness with respect to the electrolyte, because the graphene fingers are also stable when immersed into the electrolyte, as shown in Fig.3c.

By definition, AR can be improved by decreasing DA. DA is mainly occupied by the sealant needed both to assembly the device and to protect the vertical contact from the electrolyte corrosive action. It is possible to reduce the surface dedicated to the sealant by increasing the width of the cells and their number. In this way, AA increases. The layout based on Ag-interconnects comprises a finger surrounded by two sealant stripes, to avoid the electrolyte corrosion action, Figs.4a,c. The graphene-interconnects allow us to remove one sealant strip, because of the chemical resistance to the electrolyte. We thus gain space, and increase AA for the same APA, thus increasing AR.

The Ag-based DSSM comprises 5 cells (Fig.4a), each 6mm wide and 30 mm long, with 1mm wide fingers, 5mm wide inter-distance between two subsequent cells, 2 mm sealant stripes (1.1 mm at the right of the Ag finger and 1.1 mm at its left, Fig.4a). In this configuration AA=9 cm^2, DA=6 cm^2, thus APA=15 cm^2, AR=0.60. By removing the part of the sealant at the right of each finger, it is possible to accommodate both the graphene finger (1mm width as in the Ag-based device) and the AA of the cell in the same gasket (increased from 7.5 to 10 mm, Fig4.b) filled by the electrolyte.

In this first approach (Layout A, Figs.4a,b), we increase the cell width to 8mm and, consequently, DA=3 cm^2, AA=12cm^2, APA=15.6 cm^2 , AR=0.77. The sealant layout is easier to fabricate. We need only 4 areas within the green box in Fig.4b (corresponding to the APA) to protect the cells, instead of the 8 of the Ag layout in Fig.4a. The inter-distance width between two subsequent cells now is 3 mm, for the same substrate size as the Ag-based module.

In the second approach (layout B, Figs.4c,d), we increase the number of cells. The Ag-based DSSM has 5 cells, 5.5mm wide and 40 mm long, 0.8 mm finger width. The inter-distance between two subsequent cells is 4mm, 1.8 mm sealant stripes (0.9 mm at the right of the Ag finger and 0.9 mm at its left, Fig.4c). In this configuration, AA=11.1 cm^2, DA=6.4 cm^2, APA=17.40 cm^2, AR=0.63. In graphene-based devices, the

cell width is 5.5 mm and that of a finger is 0.8 mm. As in the first approach, by removing the part of the sealant at the right of each finger it is possible to enclose the graphene finger (0.8mm width) and the AA of the cell in the same gasket (increased from 6.6 to 7mm, Fig4.d), filled by the electrolyte. The change in sealant layout exploits the resistance of the graphene ink to the electrolyte. In the overall gained space, we can add one cell. Thus AA=13.2 cm^2, DA=4.2 cm^2, APA=17.40 cm^2, AR=0.76. In this case, we need only 5 areas within the green box in Fig.4d (corresponding to APA) to protect the cells, instead of the 8 of the Ag layout in Fig.4c. The inter-distance width between two subsequent cells now is 2.1 mm and we maintain the same substrate size as the Ag-based module.

We then prepare and characterize 8 devices employing both graphene and Ag-based vertical interconnects. For layout A (Figs.4a,b), we make two graphene-based devices and two Ag-based ones. The best J-V curves are in Fig.5a.

Layout A (Figs.4a,b) increases AR from 0.60 to 0.77, leading an increment of $PCE_{APA,}$ from 3.37% to 3.82% (relative increase ~12%). The slight difference (see Table 1) between the two values of J_{SC} (~1%) is due to the difference in cell width (2mm) between Ag and graphene-based devices.

Layout	Material	AR	V_{OC} (V)	J_{SC} (mA/cm^2)	FF (%)	PCE_{AA}(%)	PCE_{APA}(%)
A	**SILVER**	**0.60**	**3.54**	**-12.3**	**64.8**	**5.62**	**3.37**
A	**GRAPHENE**	**0.77**	**3.76**	**-11.2**	**61.1**	**4.96**	**3.82**
B	**SILVER**	**0.63**	**3.50**	**-11.9**	**65.3**	**5.45**	**3.43**
B	**GRAPHENE**	**0.76**	**4.47**	**-11.3**	**60.0**	**4.98**	**3.78**

Table 1: comparison between photovoltaic parameters of Ag-based DSSMs and graphene based-DSSMs for layout A (Figs.4a,b) and layout B (Figs4c,d)

I_{SC} is~22.1mA for Ag-based devices and ~26.9 mA for graphene-based ones. This significant improvement (~18%) of I_{SC} is related to the AA increase (from 9 to 12 cm^2), while maintaining the same number of cells (5).

For the 6-cells format (layout B, Figs.4c,d) we fabricate 2 graphene-based devices and 2 Ag-based, and we report the J-V curves for the best performing modules in Fig.5b. In this configuration, AR increases from 0.63 to 0.76 with respect to Ag-based devices, with a PCE_{APA} raising from 3.43 % to 3.78 % (with a relative increase~10%). J_{SC} is similar because the cell width is the same. The coupling of the electrodes is easier and faster than with Ag. Graphene-based vertical interconnects give a smoother upper surface requiring lower pressure (ΔP~-35%) and less time (Δt~-33%) for the assembling, than Ag-based ones.

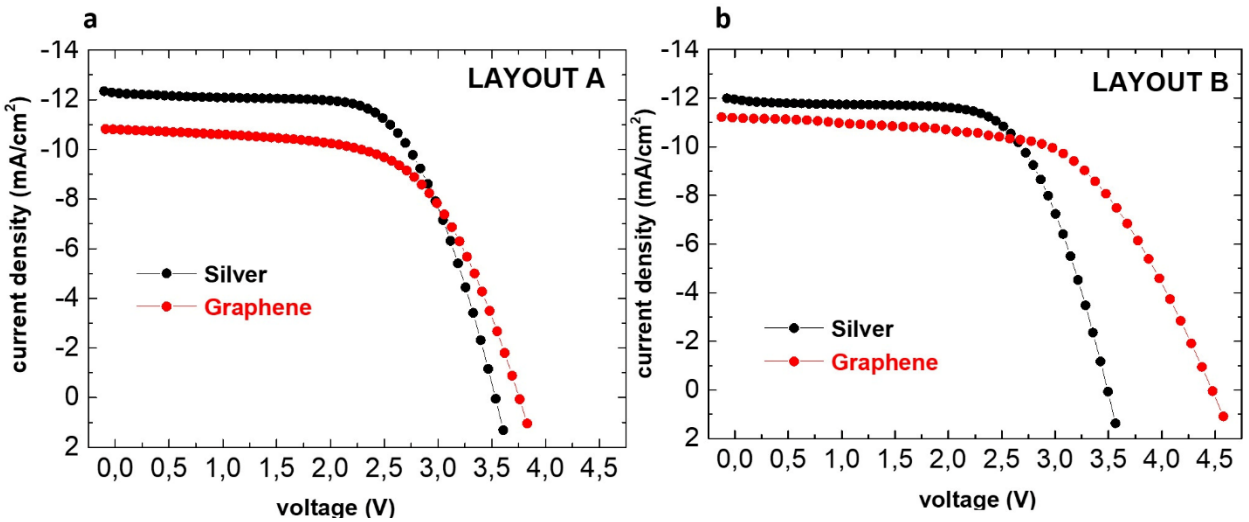

Fig. 5: Representative J-V curves for a) DSSMs layout A and b) DSSMs layout B

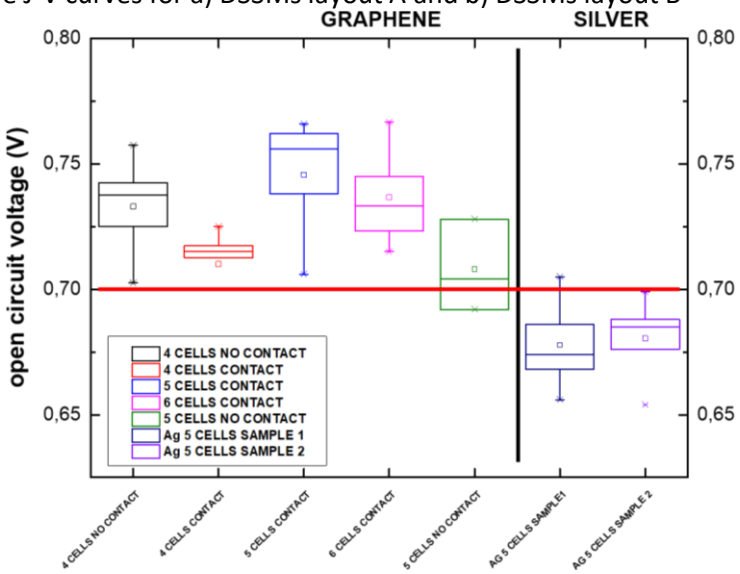

Fig.6*:* V_{OC} of different module layouts for graphene interconnects (4 cells in contact with electrolyte, 4 cells not in contact, 5 cells in contact (as for the layout in Fig.4b), 5 cells not in contact and 6 cells in contact (as for the layout in Fig.4d), and Ag interconnects (as for the layout in Figs.4a,c). To compare different configurations, V_{OC} is that of the module divided by the number of cells. The V_{OC} of modules with graphene interconnects is always higher than for Ag ones

We detect a systematic difference in V_{OC} that does not depend on module layout, as shown in Fig.6. Ag and graphene have different work functions (WF). For Ag the WF=4.26 eV,[122] for few layer graphene WF=4.7 eV.[123] Thus, the interface FTO/Ag or FTO/Graphene could induce a different voltage drop, consistent with the V_{oc} difference. The SEM images in Fig.7 show a more interconnected matrix in the case of graphene. The largest J_{sc} difference between graphene and Ag-based modules is for the A configuration. These cells have different widths: 6mm for Ag and 8mm for graphene. Thus, non-uniformity could have a larger impact for graphene modules, reducing the shunt resistance. This, combined with the increase of series resistance (wider cell) could explain the reduced current with respect to Ag. For the B configuration, statistics on J_{sc} show overlapping data. Taking into account one standard deviation, we have J_{sc}~11.7±0.4 mA/cm^2 for Ag-based devices and~11.2±0.3mA/cm^2 for graphene-based devices.

Moreover, owing to the catalytic activity of graphene,[124] we could expect some contribution to the cell current from the graphene interconnects. When these are immersed in the electrolyte, they act as an additional surface for electrolyte reduction, as the cell CE with the Pt catalyst. This, in principle, could impact the current. However, the graphene surface in contact with the electrolyte is very small, with a ratio between the two surfaces~1/200. Thus, the contribution to the current due to the graphene is negligible. The graphene electrode is porous and electrolyte can penetrate it, thus the equivalent surface (i.e. the surface contacting the electrolyte) is larger than the corresponding surface in the Ag case. The distance between graphene and PE almost one order of magnitude higher (150-200µm instead of 40µm) than between CE and PE. This results in a larger diffusion resistance, that further reduces the impact of the graphene electrode on the electrocatalysis.

For the design of a DSSM it is necessary to consider the losses due to ρ_c between FTO and printed graphene-contacts. In order to evaluate ρ_c, we measure L_T. This relates to ρ_c as:[120, 125, 126] $\rho_c = R_{FTO} \cdot L_T^2$. L_T is~0.14mm for Ag and~6.5mm for graphene. Considering the low current densities (typically~9-15mA/cm^2 for a large area series connected device)[37, 40, 127, 128] and the width of the vertical interconnects~1mm, the

photovoltaic parameters (Table 1) of graphene-based DSSMs on AA are not penalized by the higher L_T and are comparable with those of Ag-based devices. The conductivity of graphene could be improved through lithium intercalation, as discussed in Ref.[129]

The complexity of fabrication of a Z-type DSSM lies mainly in the vertical contact.[28, 48, 54, 55] The higher Ag resistance to localized deformation with respect to the thermoplastic polymer-based material used as sealant (Bynel 60, Dupont), could weaken the contact between upper and lower finger, affecting J_{SC} and FF. The presence of spikes in the printed Ag layer or the volume expansion of the electrolyte[60] could affect the sealing, separating the electrodes. At T~85°C, the distance between the two electrodes can increase because of expansion of the sealing material. If this occurs, the vertical contact could be interrupted.

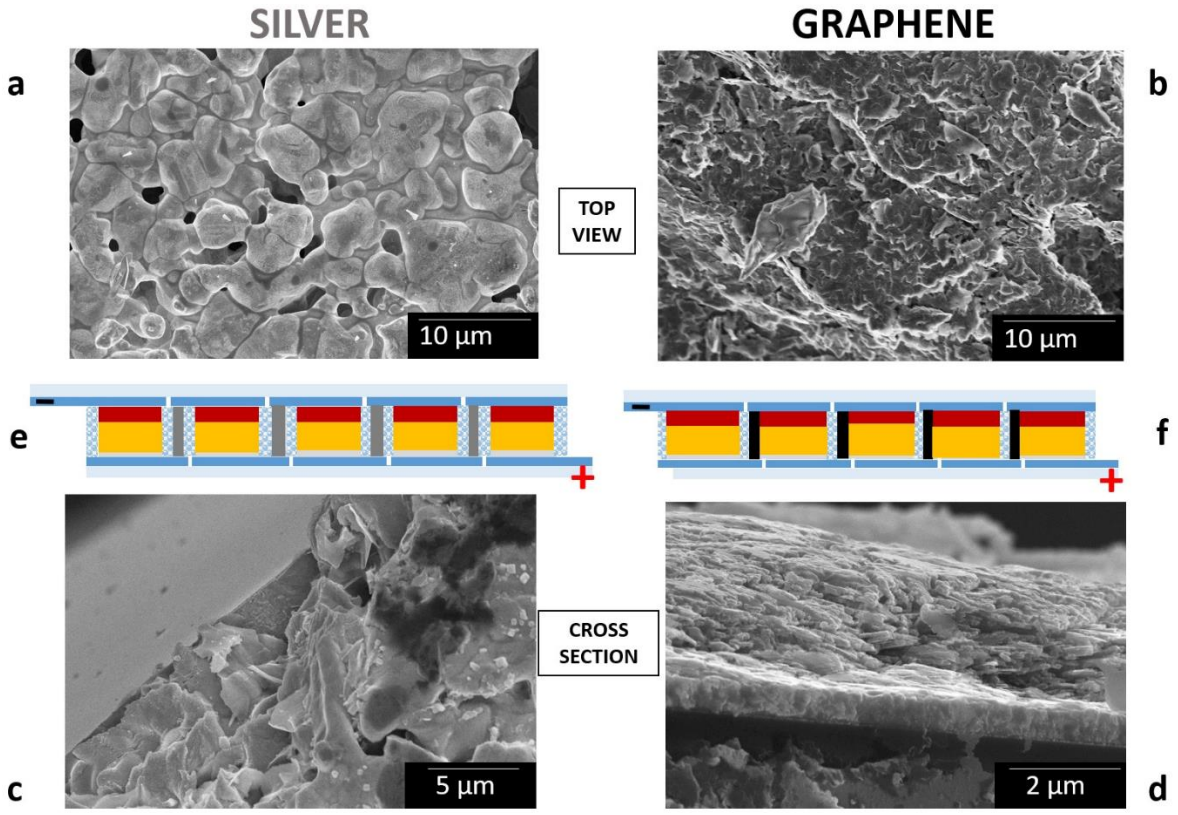

Fig.7: SEM images of: a) Ag layer, b) multi-layer graphene coating, c) cross section of Ag layer, d) cross section of multi-layer graphene coating, e) schematic cross view of Ag-based device. The structure for each vertical Ag contact is depicted in grey: cell/sealant/contact/sealant/cell,[36, 55] f) schematic cross view of graphene-based device. The structure for each vertical graphene-based contact is depicted in black: cell/sealant/contact/cell. In e,f) the TiO_2+dye layer is in red, the electrolyte in yellow, the Pt layer in clear grey, in textured blue the sealant and in simple blue the FTO.

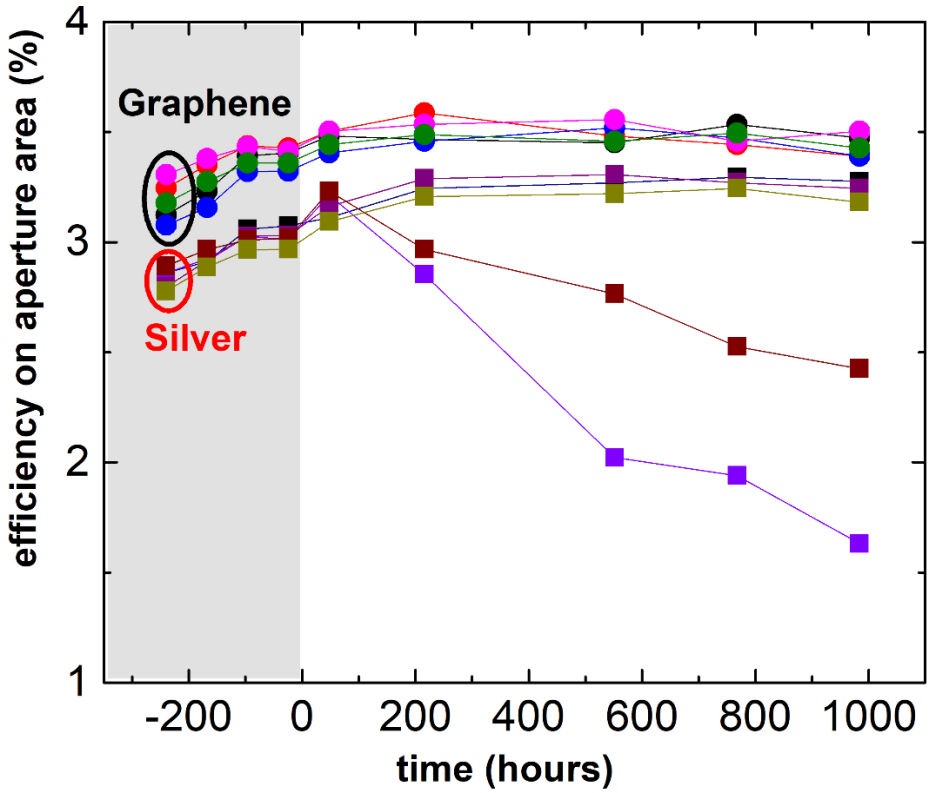

Fig. 8. Stability test at 85 °C comparing 5 DSSMs with Ag-vertical interconnects and 5 with graphene ones. Layout B (Figs.4c,d) is used. The grey region is related to the shelf life time at ambient T.

In order to avoid these issues, it is possible to deposit a layer of low T Ag paste (curing T~130°C,[130] e.g. PV412 Dupont) onto the already sintered Ag layer.[42] The deposition via screen-printing or via dispensing on one or on both substrates and curing during sealing, ensures a better contact. Mechanical pressure allows one to fill the empty spaces deriving from the roughness of the sintered Ag layers. The low T Ag paste deposition and the subsequent assembling steps must be realized very quickly (<10mins) to avoid Ag drying in air. This further step in manufacturing empathizes the complexity of fabrication. Fig.7 compares a sintered layer of Ag paste (1710, Dupont) at 480°C and a multi-layer graphene based-ink annealed at the same T. The SEM images from top of the layers shows a different agglomeration. The graphene contact appears more compact than Ag, and looks quite similar to screen-printed films for other applications, such as printed circuits.[102] SEM cross section images (Figs.7c,d) show two features for graphene layers: compactness and smoothness, when compared to Ag. The smoothness of the graphene

layers with respect to Ag, is reflected into the lower pressure needed to assemble the graphene-based modules compared to Ag ones. The morphology of graphene-based interconnects mimics the effect of the vertical contact made with the low-T Ag paste of Ref.42

These fabrication differences impact on device long-term stability. We thus perform a stability test in oven for 1000 hours at 85 °C, following the thermal stress approach of Refs.,[96, 131, 132] since DSSC technology has not yet its own certification protocols (this corresponds to ISOS-D-2 tests).[70] This is useful to assess the different behaviours of graphene and Ag-based devices, and to check the DSSMs structural stability, i.e. their robustness in terms of delamination and subsequent electrolyte leakage. For this, we fabricate and characterize 10 devices with layout B: 5 with the Ag-layout of Fig.4c, and 5 with graphene-based interconnects, with the 6-cells format in Fig.4d. In the layout of Fig.4d the vertical interconnects are not protected with an encapsulant. We use this layout to compare modules with larger AA (11.1 cm^2 for Ag-based devices and 13.2 cm^2 for graphene-based ones) and greater number of cells (in the case of graphene), in order to maximize the number of inter-distances (in the case of graphene). The graphene-based devices have a width of the strip of sealant between gasket (containing cell and one finger) and next gasket~0.8mm, Fig.4d. The number of these strips is 5. For the Ag-based devices, the strip of sealant between two gaskets, one containing only the cell, and the other containing only the finger, is~0.9mm wide. The number of these strips is 8. The surface area related to these strips is~2.88 cm^2 for Ag and~1.6 cm^2 for graphene. This means that the encapsulation is more rugged for Ag-based devices. The cell width is the same: 5.5mm. The electrolyte involved is the HSE. Before starting the thermal stress in oven, we test the devices in shelf life condition as detailed in ISOS-D-1 protocol[70] for 240h.

After 1000h at 85°C, the PCE of all graphene-based devices remains stable, Fig.8, and no structural defects, such as delamination between the two substrates, are observed. 2 out of 5 Ag-based devices have sealant delamination and subsequent electrolyte bleaching (due to contact with Ag) and leakage. Thus, graphene-based interconnects improve the structural stability of the devices.

3. CONCLUSIONS

We prepared graphene-based interconnects overcoming degradation due to corrosion of Ag grids in Z-type DSSMs. These improve the aperture area efficiency and decrease by up to~3 cm^2 the dead area (halving this value), raising by 0.17 the aspect ratio related to the substrate, with respect to devices with Ag-based interconnects. By enlarging the width of single cells or by increasing the number of cells within the same area, we achieve an enhancement of aperture area efficiency up to +12% with respect to Ag-based devices. Our approach solves two of the main issues of DSSC technology: grids corrosion and electrolyte bleaching. The graphene-based vertical interconnects increase by 40% the number of devices passing the dry heat test (1000 hours @ 85°C), underlying their effectiveness and mechanical stability, due to their intrinsic morphological characteristics, with no spikes, unlike Ag-based ones. Our work paves the way to the roll-out of DSSC technology in BIPV and for indoor applications.

4. MATERIALS AND METHODS

Graphene-ink. The ink is formulated as follows: 80 g/L of microfluidized flakes are mixed in deionized (DI) water with~9 g/L of SDC and then processed for 70 cycles with a Microfluidic processor (M-110P, Microfluidics).[102] The dispersion is then stabilised by adding at room T, while stirring, 10 g/L of carboxymethylcellulose sodium salt (CMC) as rheology modifier.[133] This allows us to reach a shear thinning viscosity as required for screen printing (~0.2 Pa·s at shear rate of $1000s^{-1}$).[102]

Dye Sensitized Solar Modules (DSSMs) and TLM. Referring both to Fig.2 and to main text, conductive substrates for DSSMs are provided from “NSG-Pilkington”. Their sheet resistance is 7 Ω sq^{-1}. They are cleaned brushing without scratching the FTO surface, using “Hellmanex” cleaning solution diluted with water in a 2:98 vol/vol ratio. Acetone and Ethanol for the ultrasonic bath (10 minutes for each of the two) are from “Sigma Aldrich”. Substrates are then rinsed in Ethanol and quickly dried with a strong air flow. The UV-O_3 treatment is performed by PSD Pro Series Digital UV Ozone System from “Novascan”. Both

etching of substrates and ablation of Ag and graphene-based contacts for TLM are performed using a "BrightSolutions, Luce 40" laser". The Ag interconnects and the graphene-based ones, the TiO_2 and Pt layers are deposited with a highly automated Screen Printer (SP) machine from "Baccini-Applied Materials". All the depositions are performed in double squeegee mode with an applied force~110 N on the screen, except for the graphene-based interconnects (in this case the applied force is~80 N). In order to screen-print both Ag and graphene-base interconnects, we use a screen with mesh 77T (i.e. 77 Threads in the polyester screen/cm). The mesh is 48T for TiO_2 and 100T for Pt. Ag paste is 7713 from "Dupont", TiO_2 paste is 18 NR-T from "Greatcell Solar" and the Pt precursor paste is from "3D-nano". Sintering, firing and drying processes are performed in oven, Lenton WHT6/60 (Hope Valley, UK). The thermal stress test is also carried out in a Lenton WHT 4/30 oven. Dye N-719 (Di-tetrabutylammonium cis-bis(isothiocyanato)bis(2,2'-bipyridyl-4,4'-dicarboxylato)ruthenium(II)) from "Sigma Aldrich" is prepared in Ethanol solution (0.3 mM). Dye DN-F05 (also known as D35CPDT, 3-4,4-dihexyl-cyclopenta-[2,1-b:3,4-b']dithiphene-2-yl}-2cyanoacrylic acid) form "Dyenamo" is prepared in Ethanol solution (0.2 mM). They are left to stir overnight before use. The electrolyte, HSE (High Stability Electrolyte) from "Greatcell Solar" is left to stir at~50°C for~20mis before use. DSSMs assembling and sealing is performed by an automated pneumatic heat press (model 50 speciale from "Memo s.r.l"), composed by two opposite heated plates. The temperature of both plates is set at T~150°C and the coupling between PE and CE is obtained using a thermoplastic foil (Bynel 60 from "Dupont") between the two electrodes. The difference of pressure between the two plates is set at~1.1bar for Ag and~0.8bar for graphene-based devices. Time of coupling is~60s for Ag and~40s for graphene-based ones. Channels for electrolyte injection (Fig.2(d2)) are sealed with UV-curable resin Threebond 3035B.

Measurements set-up. The Raman spectrum in Fig.1 is measured using a Renishaw InVia spectrometer equipped with 50x objective. The thickness of deposited materials such as Ag, graphene and TiO_2 is measured via profilometry (Deektat Veeco 150). Al the values of R_{SH} are carried out by mean of 4-point

probe system integrated in the Arkeo System from “Cicci Research”. The J-V curves of DSSMs (Fig.5) and their electrical parameters (PCE, J_{SC}, V_{OC} and FF) are acquired in air atmosphere by using a Keithley 2420 source meter coupled with a solar simulator (ABET Sun 2000, class A), calibrated by a thermopile pyranometer (Pyranometer MS-602, EKO) at AM (Air Mass) 1.5 and 100 mW cm^{-2} illumination conditions. The voltage step is 70 mV. The SEM images (Fig.6) are acquired in a Model FEI Magellan-400 XHR SEM at 15kV, 0.2 nA, with magnification 15.000-35.000.

ACKNOWLEDGMENTS

We thank V. Mirruzzo for the dye solutions and M. Ciocca for the thermoplastic masks. We acknowledge funding from the European Union's Horizon 2020 Research Innovation Program under grant agreement No GrapheneCore3 881603, the Ministry of Education and Science of the Russian Federation in the framework of Increase Competitiveness Program of NUST «MISiS» (№ К2-2019-13), ERC grant Hetero2D, EPSRC grants EP/L016087/1, EP/K01711X/1, EP/K017144/1.

REFERENCES

1. Kurtz, S. R., Leilaeioun, A., King, R. R., Peters, I. M., Heben, M. J., Metzger, W. K. & Haegel, N. M., Revisiting the Terawatt Challenge. *MRS Bull.* **45**, 159-164 (2020).

2. IEA, Installed power generation capacity by source in the Stated Policies Scenario, 2000-2040, IEA, Paris. [cited]; Available from: https://www.iea.org/data-and-statistics/charts/installed-power-generation-capacity-by-source-in-the-stated-policies-scenario-2000-2040

3. Grätzel, M., Dye-sensitized solar cells. *Journal of Photochemistry and Photobiology C: Photochemistry Reviews* **4**, 145-153 (2003).

4. Nazeeruddin, M. K., Baranoff, E. & Grätzel, M., Dye-sensitized solar cells: A brief overview. *Solar Energy* **85**, 1172-1178 (2011).

5. Grätzel, M., Photoelectrochemical cells. *Nature* **414**, 338-344 (2001).

6. Lee, H. M. & Yoon, J. H., Power performance analysis of a transparent DSSC BIPV window based on 2 year measurement data in a full-scale mock-up. *Applied Energy* **225**, 1013-1021 (2018).

7. Freitas, S. & Brito, M. C., Solar façades for future cities. *Renewable Energy Focus* **31**, 73-79 (2019).

8. Selvaraj, P., Ghosh, A., Mallick, T. K. & Sundaram, S., Investigation of semi-transparent dye-sensitized solar cells for fenestration integration. *Renewable Energy* **141**, 516-525 (2019).

9. Freitag, M., Teuscher, J., Saygili, Y., Zhang, X., Giordano, F., Liska, P., Hua, J., Zakeeruddin, S. M., Moser, J.-E., Grätzel, M. & Hagfeldt, A., Dye-sensitized solar cells for efficient power generation under ambient lighting. *Nature Photonics* **11**, 372-378 (2017).

10. Hagfeldt, A., Boschloo, G., Sun, L., Kloo, L. & Pettersson, H., Dye-Sensitized Solar Cells. *Chem. Rev.* **110**, 6595-6663 (2010).

11. Lai, F.-I., Yang, J.-F., Hsu, Y.-C. & Kuo, S.-Y., Omnidirectional light harvesting enhancement of dye-sensitized solar cells decorated with two-dimensional ZnO nanoflowers. *J. Alloys Compd.* **815**, 152287 (2020).

12. Nayak, P. K., Mahesh, S., Snaith, H. J. & Cahen, D., Photovoltaic solar cell technologies: analysing the state of the art. *Nature Reviews Materials* **4**, 269-285 (2019).

13. Khanna, S., Sundaram, S., Reddy, K. S. & Mallick, T. K., Performance analysis of perovskite and dye-sensitized solar cells under varying operating conditions and comparison with monocrystalline silicon cell. *Appl. Therm. Eng.* **127**, 559-565 (2017).

14. Kaplani, E. & Kaplanis, S., Thermal modelling and experimental assessment of the dependence of PV module temperature on wind velocity and direction, module orientation and inclination. *Solar Energy* **107**, 443-460 (2014).

15. Husain, A. A. F., Hasan, W. Z. W., Shafie, S., Hamidon, M. N. & Pandey, S. S., A review of transparent solar photovoltaic technologies. *Renewable and Sustainable Energy Reviews* **94**, 779-791 (2018).

16. Tagliaferro, R., Colonna, D., Brown, T. M., Reale, A. & Di Carlo, A., Interplay between transparency and efficiency in dye sensitized solar cells. *Opt. Express* **21**, 3235-3242 (2013).

17. Pulli, E., Rozzi, E. & Bella, F., Transparent photovoltaic technologies: Current trends towards upscaling. *Energy Convers. Manage.* **219**, 112982 (2020).

18. Sharma, K., Sharma, V. & Sharma, S., Dye-sensitized solar cells: fundamentals and current status. *Nanoscale research letters* **13**, 381 (2018).

19. Thomas, S., Deepak, T. G., Anjusree, G. S., Arun, T. A., Nair, S. V. & Nair, A. S., A review on counter electrode materials in dye-sensitized solar cells. *J. Mater. Chem. A* **2**, 4474-4490 (2014).

20. Wu, M., Sun, M., Zhou, H., Ma, J.-Y. & Ma, T., Carbon Counter Electrodes in Dye-Sensitized and Perovskite Solar Cells. *Adv. Funct. Mater.* **30**, 1906451 (2020).

21. Ardo, S. & Meyer, G. J., Photodriven heterogeneous charge transfer with transition-metal compounds anchored to TiO2 semiconductor surfaces. *Chem. Soc. Rev.* **38**, 115-164 (2009).

22. Paulose, M., Shankar, K., Varghese, O. K., Mor, G. K., Hardin, B. & Grimes, C. A., Backside illuminated dye-sensitized solar cells based on titania nanotube array electrodes. *Nanotechnology* **17**, 1446 (2006).

23. O'Regan, B. & Grätzel, M., A low-cost, high-efficiency solar cell based on dye-sensitized colloidal TiO2 films. *Nature* **353**, 737-740 (1991).

24. Anderson, S., Constable, E. C., Dare-Edwards, M. P., Goodenough, J. B., Hamnett, A., Seddon, K. R. & Wright, R. D., Chemical modification of a titanium (IV) oxide electrode to give stable dye sensitisation without a supersensitiser. *Nature* **280**, 571-573 (1979).

25. Gong, J., Liang, J. & Sumathy, K., Review on dye-sensitized solar cells (DSSCs): Fundamental concepts and novel materials. *Renewable and Sustainable Energy Reviews* **16**, 5848-5860 (2012).

26. Iftikhar, H., Sonai, G. G., Hashmi, S. G., Nogueira, A. F. & Lund, P. D. Progress on Electrolytes Development in Dye-Sensitized Solar Cells. *Materials (Basel, Switzerland)*; 2019.

27. Mariani, P., Vesce, L. & Di Carlo, A., The role of printing techniques for large-area dye sensitized solar cells. *Semicond. Sci. Technol.* **30**, 104003 (2015).

28. Vesce, L., Guidobaldi, A., Mariani, P., Di Carlo, A., Parisi, M. L., Maranghi, S. & Basosi, R. Scaling-up of Dye Sensitized Solar Modules. *World Scientific Reference of Hybrid Materials*. World Scientific, 2019, pp 423-485.

29. Ramasamy, E., Lee, W. J., Lee, D. Y. & Song, J. S., Portable, parallel grid dye-sensitized solar cell module prepared by screen printing. *J. Power Sources* **165**, 446-449 (2007).

30. Zhang, J., Lin, H., Li, J. B., Li, X. & Zhao, X. C., DSCs Modules Fabricated by Screen Printing. *Key Eng. Mater.* **434-435**, 638-641 (2010).

31. Dai, S., Wang, K., Weng, J., Sui, Y., Huang, Y., Xiao, S., Chen, S., Hu, L., Kong, F. & Pan, X., Design of DSC panel with efficiency more than 6%. *Sol. Energy Mater. Sol. Cells* **85**, 447-455 (2005).

32. Escalante, R., Pourjafari, D., Reyes-Coronado, D. & Oskam, G., Dye-sensitized solar cell scale-up: Influence of substrate resistance. *Journal of Renewable and Sustainable Energy* **8**, 023704 (2016).

33. Takeda, Y., Kato, N., Higuchi, K., Takeichi, A., Motohiro, T., Fukumoto, S., Sano, T. & Toyoda, T., Monolithically series-interconnected transparent modules of dye-sensitized solar cells. *Sol. Energy Mater. Sol. Cells* **93**, 808-811 (2009).

34. Pettersson, H., Gruszecki, T., Schnetz, C., Streit, M., Xu, Y., Sun, L., Gorlov, M., Kloo, L., Boschloo, G., Häggman, L. & Hagfeldt, A., Parallel-connected monolithic dye-sensitised solar modules. *Progress in Photovoltaics: Research and Applications* **18**, 340-345 (2010).

35. Atsushi, F., Nobuhiro, F., Ryoichi, K., Naoki, K., Ryohsuke, Y., Hiroyuki, K. & Liyuan, H., Dye-Sensitized Photovoltaic Module with Conversion Efficiency of 8.4%. *Applied Physics Express* **2**, 082202 (2009).

36. Han, L., Fukui, A., Chiba, Y., Islam, A., Komiya, R., Fuke, N., Koide, N., Yamanaka, R. & Shimizu, M., Integrated dye-sensitized solar cell module with conversion efficiency of 8.2%. *Appl. Phys. Lett.* **94**, 013305 (2009).

37. Sastrawan, R., Beier, J., Belledin, U., Hemming, S., Hinsch, A., Kern, R., Vetter, C., Petrat, F., Prodi-Schwab, A. & Lechner, P., A glass frit-sealed dye solar cell module with integrated series connections. *Sol. Energy Mater. Sol. Cells* **90**, 1680-1691 (2006).

38. Kim, H., Jo, J., Lee, G., Shin, M. & Lee, J.-C., Design and analysis of a highly reliable large-area Z-type transparent module for dye-sensitized solar cells. *Solar Energy* **155**, 585-592 (2017).

39. Toyoda, T., Sano, T., Nakajima, J., Doi, S., Fukumoto, S., Ito, A., Tohyama, T., Yoshida, M., Kanagawa, T., Motohiro, T., Shiga, T., Higuchi, K., Tanaka, H., Takeda, Y., Fukano, T., Katoh, N., Takeichi, A., Takechi, K. & Shiozawa, M., Outdoor performance of large scale DSC modules. *J. Photochem. Photobiol. A: Chem.* **164**, 203-207 (2004).

40. Giordano, F., Guidobaldi, A., Petrolati, E., Vesce, L., Riccitelli, R., Reale, A., Brown, T. M. & Di Carlo, A., Realization of high performance large area Z-series-interconnected opaque dye solar cell modules. *Progress in Photovoltaics: Research and Applications* **21**, 1653-1658 (2013).

41. Giordano, F., Petrolati, E., Brown, T. M., Reale, A. & Di Carlo, A., Series-connection designs for dye solar cell modules. *Electron Devices, IEEE Transactions on* **58**, 2759-2764 (2011).

42. Giordano, F., Pretrolati, E., Guidobaldi, A., Brown, T. & Tozzi, R. Vertical electrical connection of photoelectrochemical cells. Google Patents; 2013.

43. Reale, A., Cinà, L., Malatesta, A., Marco, R., Brown, T. & Di Carlo, A., Estimation of Energy Production of Dye-Sensitized Solar Cell Modules for Building-Integrated Photovoltaic Applications. *Energy Technology* **2**, (2014).

44. Green, M. A., Dunlop, E. D., Hohl-Ebinger, J., Yoshita, M., Kopidakis, N. & Hao, X., Solar cell efficiency tables (version 56). *Progress in Photovoltaics: Research and Applications* **28**, 629-638 (2020).

45. Palma, A. L., Matteocci, F., Agresti, A., Pescetelli, S., Calabrò, E., Vesce, L., Christiansen, S., Schmidt, M. & Carlo, A. D., Laser-Patterning Engineering for Perovskite Solar Modules With 95% Aperture Ratio. *IEEE Journal of Photovoltaics* **7**, 1674-1680 (2017).

46. Castro-Hermosa, S., Yadav, S. K., Vesce, L., Guidobaldi, A., Reale, A., Carlo, A. D. & Brown, T. M., Stability issues pertaining large area perovskite and dye-sensitized solar cells and modules. *Journal of Physics D: Applied Physics* **50**, 033001 (2017).

47. Hashmi, G., Miettunen, K., Peltola, T., Halme, J., Asghar, I., Aitola, K., Toivola, M. & Lund, P., Review of materials and manufacturing options for large area flexible dye solar cells. *Renewable and Sustainable Energy Reviews* **15**, 3717-3732 (2011).

48. Fakharuddin, A., Jose, R., Brown, T. M., Fabregat-Santiago, F. & Bisquert, J., A perspective on the production of dye-sensitized solar modules. *Energy & Environmental Science* **7**, 3952-3981 (2014).

49. Sastrawan, R., Beier, J., Belledin, U., Hemming, S., Hinsch, A., Kern, R., Vetter, C., Petrat, F. M., Prodi-Schwab, A., Lechner, P. & Hoffmann, W., New interdigital design for large area dye solar modules using a lead-free glass frit sealing. *Progress in Photovoltaics: Research and Applications* **14**, 697-709 (2006).

50. Green, M. A., Accuracy of analytical expressions for solar cell fill factors. *Solar Cells* **7**, 337-340 (1982).

51. Jun, Y., Son, J.-H., Sohn, D. & Kang, M. G., A module of a TiO2 nanocrystalline dye-sensitized solar cell with effective dimensions. *J. Photochem. Photobiol. A: Chem.* **200**, 314-317 (2008).

52. Ahn, S.-H., Choi, J.-O., Kim, C.-S., Lee, G.-Y., Lee, H.-T., Cho, K., Chun, D.-M. & Lee, C. S., Laser-assisted nano particle deposition system and its application for dye sensitized solar cell fabrication. *CIRP Annals-Manufacturing Technology* **61**, 575-578 (2012).

53. Vesce, L., Riccitelli, R., Soscia, G., Brown, T. M., Di Carlo, A. & Reale, A., Optimization of nanostructured titania photoanodes for dye-sensitized solar cells: study and experimentation of TiCl 4 treatment. *J. Non-Cryst. Solids* **356**, 1958-1961 (2010).

54. Wang, M., Chamberland, N., Breau, L., Moser, J.-E., Humphry-Baker, R., Marsan, B., Zakeeruddin, S. M. & Grätzel, M., An organic redox electrolyte to rival triiodide/iodide in dye-sensitized solar cells. *Nature Chemistry* **2**, 385-389 (2010).

55. Wang, L., Fang, X. & Zhang, Z., Design methods for large scale dye-sensitized solar modules and the progress of stability research. *Renewable and Sustainable Energy Reviews* **14**, 3178-3184 (2010).

56. Fukui, A., Fuke, N., Komiya, R., Koide, N., Yamanaka, R., Katayama, H. & Han, L., Dye-Sensitized Photovoltaic Module with Conversion Efficiency of 8.4%. *Applied Physics Express* **2**, 082202 (2009).

57. Miettunen, K., Etula, J., Saukkonen, T., Jouttijärvi, S., Halme, J., Romu, J. & Lund, P., Insights into corrosion in dye solar cells. *Progress in Photovoltaics: Research and Applications* **23**, 1045-1056 (2015).

58. Sommeling, P. M., Späth, M., Smit, H., Bakker, N. & Kroon, J., Long-term stability testing of dye-sensitized solar cells. *J. Photochem. Photobiol. A: Chem.* **164**, 137-144 (2004).

59. Sawada, M. & Nagakane, T., inventors; Google Patents, assignee. Glass substrate with conductive film for solar cell. Patent US8871348 B2. 2014.

60. Han, C., Park, S. & Oh, W., Reliability-based structural optimization of 300 × 300 mm 2 dye-sensitized solar cell module. *Solar Energy* **150**, 128-135 (2017).

61. Mastroianni, S., Asghar, I., Miettunen, K., Halme, J., Lanuti, A., Brown, T. M. & Lund, P., Effect of electrolyte bleaching on the stability and performance of dye solar cells. *PCCP* **16**, 6092-6100 (2014).

62. Asghar, M. I., Miettunen, K., Halme, J., Vahermaa, P., Toivola, M., Aitola, K. & Lund, P., Review of stability for advanced dye solar cells. *Energy & Environmental Science* **3**, 418-426 (2010).

63. Jiang, N., Sumitomo, T., Lee, T., Pellaroque, A., Bellon, O., Milliken, D. & Desilvestro, H. *High temperature stability of dye solar cells*, vol. 119, 2013.

64. Späth, M., Sommeling, P., Van Roosmalen, J., Smit, H., Van der Burg, N., Mahieu, D., Bakker, N. & Kroon, J., Reproducible manufacturing of dye-sensitized solar cells on a semi-automated baseline. *Progress in Photovoltaics: Research and applications* **11**, 207-220 (2003).

65. Ivanou, D. K., Santos, R., Maçaira, J., Andrade, L. & Mendes, A., Laser assisted glass frit sealing for production large area DSCs panels. *Solar Energy* **135**, 674-681 (2016).

66. Casaluci, S., Gemmi, M., Pellegrini, V., Di Carlo, A. & Bonaccorso, F., Graphene-based large area dye-sensitized solar cell module. *Nanoscale*, (2016).

67. Mariani, P., Vesce, L. & Carlo, A. D. A novel class of dye-sensitized solar modules. Glass-plastic structure for mechanically stable devices. 2018 IEEE 4th International Forum on Research and Technology for Society and Industry (RTSI); 2018 10-13 Sept. 2018; 2018. p. 1-5.

68. Lee, W. J., Ramasamy, E., Lee, D. Y. & Song, J. S., Glass frit overcoated silver grid lines for nano-crystalline dye sensitized solar cells. *J. Photochem. Photobiol. A: Chem.* **183**, 133-137 (2006).

69. Gorni, G., Zama, I., Martelli, C. & Armiento, L., Fabrication of dye-sensitized solar modules based on a prototyping pilot line and their integration into energy storage microsystems. *J. Eur. Ceram. Soc.*, (2017).

70. Reese, M. O., Gevorgyan, S. A., Jørgensen, M., Bundgaard, E., R., K. S., Ginley, D. S., Olson, D. C., Lloyd, M. T., Morvillo, P., A., K. E., Elschner, A., Haillant, O., Currier, T. R., Shrotriya, V., Hermenau, M., Riede, M., Kirov, K. R., Trimmel, G., Rath, T., Inganas, O., Zhang, F., Andersson, M., Tvingstedt, K., Lira-Cantu, M., Laird, D., McGuiness, C., Gowrisanker, S. J., Pannone, M., Xiao, M., Hauch, J., Steim, R., DeLongchamp, D. M., Rosch, R., Hoppe, H., Espinosa, N., Urbina, A., Yaman-Uzunoglu, G., Bonekamp, J.-B., van Breemen, A. J. J. M., Girotto, C., Voroshazi, E. & Krebs, F. C., Consensus stability testing protocols for organic photovoltaic materials and devices. *Sol. Energy Mater. Sol. Cells* **95**, 1253–1267 (2011).

71. Khenkin, M. V., Katz, E. A., Abate, A., Bardizza, G., Berry, J. J., Brabec, C., Brunetti, F., Bulović, V., Burlingame, Q., Di Carlo, A., Cheacharoen, R., Cheng, Y.-B., Colsmann, A., Cros, S., Domanski, K., Dusza, M., Fell, C. J., Forrest, S. R., Galagan, Y., Di Girolamo, D., Grätzel, M., Hagfeldt, A., von Hauff, E., Hoppe, H., Kettle, J., Köbler, H., Leite, M. S., Liu, S., Loo, Y.-L., Luther, J. M., Ma, C.-Q., Madsen, M., Manceau, M., Matheron, M., McGehee, M., Meitzner, R., Nazeeruddin, M. K., Nogueira, A. F., Odabaşı, Ç., Osherov, A., Park, N.-G., Reese, M. O., De Rossi, F., Saliba, M., Schubert, U. S., Snaith, H. J., Stranks, S. D., Tress, W., Troshin, P. A., Turkovic, V., Veenstra, S., Visoly-Fisher, I., Walsh, A., Watson, T., Xie, H., Yıldırım, R., Zakeeruddin, S. M., Zhu, K. & Lira-Cantu, M., Consensus statement for stability assessment and reporting for perovskite photovoltaics based on ISOS procedures. *Nature Energy* **5**, 35-49 (2020).

72. Hopkins, J. A., Phani, G. & Skryabin, I. L. Methods to implement interconnects in multi-cell regenerative photovoltaic photoelectrochemical devices. Google Patents; 2000.

73. Tulloch, G. & Skryabin, I. Photoelectrochemical device. Google Patents; 2006.

74. Ito, S., Zakeeruddin, S. M., Comte, P., Liska, P., Kuang, D. & Grätzel, M., Bifacial dye-sensitized solar cells based on an ionic liquid electrolyte. *Nature Photonics* **2**, 693-698 (2008).

75. Venkatesan, S., Lin, W.-H., Teng, H. & Lee, Y.-L., High-Efficiency Bifacial Dye-Sensitized Solar Cells for Application under Indoor Light Conditions. *ACS Applied Materials & Interfaces* **11**, 42780-42789 (2019).

76. Bonaccorso, F., Sun, Z., Hasan, T. & Ferrari, A. C., Graphene photonics and optoelectronics. *Nature Photonics* **4**, 611-622 (2010).

77. Ferrari, A. C., Bonaccorso, F., Fal'ko, V., Novoselov, K. S., Roche, S., Bøggild, P., Borini, S., Koppens, F. H. L., Palermo, V., Pugno, N., Garrido, J. A., Sordan, R., Bianco, A., Ballerini, L., Prato, M., Lidorikis, E., Kivioja, J., Marinelli, C., Ryhänen, T., Morpurgo, A., Coleman, J. N., Nicolosi, V., Colombo, L., Fert, A., Garcia-Hernandez, M., Bachtold, A., Schneider, G. F., Guinea, F., Dekker, C., Barbone, M., Sun, Z., Galiotis, C., Grigorenko, A. N., Konstantatos, G., Kis, A., Katsnelson, M., Vandersypen, L., Loiseau, A., Morandi, V., Neumaier, D., Treossi, E., Pellegrini, V., Polini, M., Tredicucci, A., Williams, G. M., Hee Hong, B., Ahn, J.-H., Min Kim, J., Zirath, H., van Wees, B. J., van der Zant, H., Occhipinti, L., Di Matteo, A., Kinloch, I. A., Seyller, T., Quesnel, E., Feng, X., Teo, K., Rupesinghe, N., Hakonen, P., Neil, S. R. T., Tannock, Q., Löfwander, T. & Kinaret, J., Science and technology roadmap for graphene, related two-dimensional crystals, and hybrid systems. *Nanoscale* **7**, 4598-4810 (2015).

78. Won, R., Graphene–silicon solar cells. *Nature Photonics* **4**, 411-411 (2010).

79. Kong, X., Zhang, L., Liu, B., Gao, H., Zhang, Y., Yan, H. & Song, X., Graphene/Si Schottky solar cells: a review of recent advances and prospects. *RSC Advances* **9**, 863-877 (2019).

80. Lin, X.-F., Zhang, Z.-Y., Yuan, Z.-K., Li, J., Xiao, X.-F., Hong, W., Chen, X.-D. & Yu, D.-S., Graphene-based materials for polymer solar cells. *Chin. Chem. Lett.* **27**, 1259-1270 (2016).

81. Wu, J., Becerril, H. A., Bao, Z., Liu, Z., Chen, Y. & Peumans, P., Organic solar cells with solution-processed graphene transparent electrodes. *Appl. Phys. Lett.* **92**, 263302 (2008).

82. Bouclé, J. & Herlin-Boime, N., The benefits of graphene for hybrid perovskite solar cells. *Synth. Met.* **222**, 3-16 (2016).

83. Lim, E. L., Yap, C., Hj. Jumali, M., Mat Teridi, M. A. & Teh, C. H., A Mini Review: Can Graphene Be a Novel Material for Perovskite Solar Cell Applications? *Nano-Micro Letters* **10**, 27 (2017).

84. Agresti, A., Pescetelli, S., Palma, A. L., Del Rio Castillo, A. E., Konios, D., Kakavelakis, G., Razza, S., Cinà, L., Kymakis, E., Bonaccorso, F. & Di Carlo, A., Graphene Interface Engineering for Perovskite Solar Modules: 12.6% Power Conversion Efficiency over 50 cm2 Active Area. *ACS Energy Letters* **2**, 279-287 (2017).

85. Agresti, A., Pescetelli, S., Taheri, B., Del Rio Castillo, A. E., Cinà, L., Bonaccorso, F. & Di Carlo, A., Graphene–Perovskite Solar Cells Exceed 18 % Efficiency: A Stability Study. *ChemSusChem* **9**, 2609-2619 (2016).

86. Agresti, A., Pescetelli, S., Palma, A. L., Martín-García, B., Najafi, L., Bellani, S., Moreels, I., Prato, M., Bonaccorso, F. & Di Carlo, A., Two-Dimensional Material Interface Engineering for Efficient Perovskite Large-Area Modules. *ACS Energy Letters* **4**, 1862-1871 (2019).

87. Agresti, A., Pescetelli, S., Cinà, L., Konios, D., Kakavelakis, G., Kymakis, E. & Carlo, A. D., Efficiency and Stability Enhancement in Perovskite Solar Cells by Inserting Lithium-Neutralized Graphene Oxide as Electron Transporting Layer. *Adv. Funct. Mater.* **26**, 2686-2694 (2016).

88. Palma, A. L., Cinà, L., Pescetelli, S., Agresti, A., Raggio, M., Paolesse, R., Bonaccorso, F. & Di Carlo, A., Reduced graphene oxide as efficient and stable hole transporting material in mesoscopic perovskite solar cells. *Nano Energy* **22**, 349-360 (2016).

89. Roy-Mayhew, J. D. & Aksay, I. A., Graphene Materials and Their Use in Dye-Sensitized Solar Cells. *Chem. Rev.* **114**, 6323-6348 (2014).

90. Singh, E. & Nalwa, H. S., Graphene-Based Dye-Sensitized Solar Cells: A Review. *Science of Advanced Materials* **9**, 1863-1912 (2015).

91. Wang, H. & Hu, Y. H., Graphene as a counter electrode material for dye-sensitized solar cells. *Energy & Environmental Science* **5**, 8182-8188 (2012).

92. Kavan, L., Yum, J. H. & Grätzel, M., Optically Transparent Cathode for Dye-Sensitized Solar Cells Based on Graphene Nanoplatelets. *ACS Nano* **5**, 165-172 (2011).

93. Hong, W., Xu, Y., Lu, G., Li, C. & Shi, G., Transparent graphene/PEDOT–PSS composite films as counter electrodes of dye-sensitized solar cells. *Electrochem. Commun.* **10**, 1555-1558 (2008).

94. Durantini, J., Boix, P. P., Gervaldo, M., Morales, G. M., Otero, L., Bisquert, J. & Barea, E. M., Photocurrent enhancement in dye-sensitized photovoltaic devices with titania–graphene composite electrodes. *J. Electroanal. Chem.* **683**, 43-46 (2012).

95. Kang, M. G., Park, N.-G., Park, Y. J., Ryu, K. S. & Chang, S. H., Manufacturing method for transparent electric windows using dye-sensitized TiO2 solar cells. *Sol. Energy Mater. Sol. Cells* **75**, 475-479 (2003).

96. Yadav, S. K., Ravishankar, S., Pescetelli, S., Agresti, A., Fabregat-Santiago, F. & Di Carlo, A., Stability of dye-sensitized solar cells under extended thermal stress. *PCCP* **19**, 22546-22554 (2017).

97. Peter, L., "Sticky Electrons" Transport and Interfacial Transfer of Electrons in the Dye-Sensitized Solar Cell. *Acc. Chem. Res.* **42**, 1839-1847 (2009).

98. Yang, N., Zhai, J., Wang, D., Chen, Y. & Jiang, L., Two-Dimensional Graphene Bridges Enhanced Photoinduced Charge Transport in Dye-Sensitized Solar Cells. *ACS Nano* **4**, 887-894 (2010).

99. Selopal, G. S., Milan, R., Ortolani, L., Morandi, V., Rizzoli, R., Sberveglieri, G., Veronese, G. P., Vomiero, A. & Concina, I., Graphene as transparent front contact for dye sensitized solar cells. *Solar Energy Materials and Solar Cells* **135**, 99-105 (2015).

100. Velten, J. A., Carretero-González, J., Castillo-Martínez, E., Bykova, J., Cook, A., Baughman, R. & Zakhidov, A., Photoinduced Optical Transparency in Dye-Sensitized Solar Cells Containing Graphene Nanoribbons. *The Journal of Physical Chemistry C* **115**, 25125-25131 (2011).

101. Kundu, S., Sarojinijeeva, P., Karthick, R., Anantharaj, G., Saritha, G., Bera, R., Anandan, S., Patra, A., Ragupathy, P., Selvaraj, M., Jeyakumar, D. & Pillai, K. V., Enhancing the Efficiency of DSSCs by the Modification of TiO2 Photoanodes using N, F and S, co-doped Graphene Quantum Dots. *Electrochim. Acta* **242**, 337-343 (2017).

102. Karagiannidis, P. G., Hodge, S. A., Lombardi, L., Tomarchio, F., Decorde, N., Milana, S., Goykhman, I., Su, Y., Mesite, S. V., Johnstone, D. N., Leary, R. K., Midgley, P. A., Pugno,

N. M., Torrisi, F. & Ferrari, A. C., Microfluidization of Graphite and Formulation of Graphene-Based Conductive Inks. *ACS Nano* **11**, 2742-2755 (2017).

103. Panagiotou, T., Mesite, S., Bernard, J., Chomistek, K. & Fisher, R., Production of Polymer Nanosuspensions Using Microfluidizer® Processor Based Technologies. (2008).

104. Hasan, T., Torrisi, F., Sun, Z., Popa, D., Nicolosi, V., Privitera, G., Bonaccorso, F. & Ferrari, A. C., Solution-phase exfoliation of graphite for ultrafast photonics. *physica status solidi (b)* **247**, 2953-2957 (2010).

105. Lotya, M., Hernandez, Y., King, P. J., Smith, R. J., Nicolosi, V., Karlsson, L. S., Blighe, F. M., De, S., Wang, Z., McGovern, I. T., Duesberg, G. S. & Coleman, J. N., Liquid Phase Production of Graphene by Exfoliation of Graphite in Surfactant/Water Solutions. *JACS* **131**, 3611-3620 (2009).

106. Paton, K. R., Varrla, E., Backes, C., Smith, R. J., Khan, U., O'Neill, A., Boland, C., Lotya, M., Istrate, O. M., King, P., Higgins, T., Barwich, S., May, P., Puczkarski, P., Ahmed, I., Moebius, M., Pettersson, H., Long, E., Coelho, J., O'Brien, S. E., McGuire, E. K., Sanchez, B. M., Duesberg, G. S., McEvoy, N., Pennycook, T. J., Downing, C., Crossley, A., Nicolosi, V. & Coleman, J. N., Scalable production of large quantities of defect-free few-layer graphene by shear exfoliation in liquids. *Nature Materials* **13**, 624-630 (2014).

107. Microfluidicscorp™. [cited September 10, 2017]; Available from: https://www.microfluidicscorp.com

108. Ferrari, A. C. & Basko, D. M., Raman spectroscopy as a versatile tool for studying the properties of graphene. *Nature Nanotechnology* **8**, 235–246 (2013).

109. Vig, J. R., UV/ozone cleaning of surfaces. *Journal of Vacuum Science & Technology A* **3**, 1027-1034 (1985).

110. Huang, L., Hu, Z., Xu, J., Sun, X., Du, Y., Ni, J., Cai, H., Li, J. & Zhang, J., Efficient electron-transport layer-free planar perovskite solar cells via recycling the FTO/glass substrates from degraded devices. *Sol. Energy Mater. Sol. Cells* **152**, 118-124 (2016).

111. Vesce, L. & Riccitelli, R., Processing and characterization of a TiO2 paste based on small particle size powders for dye-sensitized solar cell semi-transparent photo-electrodes. *Progress in Photovoltaics: Research and Applications* **20**, 960-966 (2012).

112. Baglio, V., Girolamo, M., Antonucci, V. & Aricò, A. S., Influence of TiO2 Film Thickness on the Electrochemical Behaviour of Dye-Sensitized Solar Cells. *International Journal of Electrochemical Science* **6**, 3375-3384 (2011).

113. Kumari, K., Sanjeevadharshini, N., Dissanayake, L., Senadeera, G. K. R. & Thotawatthage, C., The effect of TiO2 photo anode film thickness on photovoltaic properties of dye-sensitized solar cells. *Ceylon Journal of Science* **45**, 33 (2016).

114. Kalyanasundaram, K. *Dye-sensitized solar cells*. EPFL press, 2010.

115. Lin, F.-S., Priyanka, P., Fan, M.-S., Vegiraju, S., Ni, J.-S., Wu, Y.-C., Li, Y.-H., Lee, G.-H., Ezhumalai, Y., Jeng, R.-J., Chen, M.-C. & Ho, K.-C., Metal-free efficient dye-sensitized solar cells based on thioalkylated bithiophenyl organic dyes. *J. Mater. Chem. C* **8**, 15322-15330 (2020).

116. Mariotti, N., Bonomo, M., Fagiolari, L., Barbero, N., Gerbaldi, C., Bella, F. & Barolo, C., Recent advances in eco-friendly and cost-effective materials towards sustainable dye-sensitized solar cells. *Green Chemistry*, (2020).

117. Ito, S., Murakami, T. N., Comte, P., Liska, P., Grätzel, C., Nazeeruddin, M. K. & Grätzel, M., Fabrication of thin film dye sensitized solar cells with solar to electric power conversion efficiency over 10%. *Thin Solid Films* **516**, 4613-4619 (2008).

118. Vinod, P. N., Specific contact resistance measurements of the screen-printed Ag thick film contacts in the silicon solar cells by three-point probe methodology and TLM method. *Journal of Materials Science: Materials in Electronics* **22**, 1248-1257 (2011).

119. Shockley, W. Theory and Experiment on Current Transfer from Alloyed Contact to Diffused Layer. *Research and Investigation of Inverse Epitaxial UHF Power Transistors - Technical Documentary Report No. AL TDR 64-207 - Appendix B*. A. Goetzberger, R. M. Scarlett, AF Avionics Laboratory - Research and Technology Division, Wright-Patterson Air Force Base – Ohio, 1964, pp 113-130.

120. Reeves, G. K. & Harrison, H. B., Obtaining the specific contact resistance from transmission line model measurements. *IEEE Electron Device Lett.* **3**, 111-113 (1982).

121. Zhao, J., Wu, J., Zheng, M., Huo, J. & Tu, Y., Improving the photovoltaic performance of dye-sensitized solar cell by graphene/titania photoanode. *Electrochim. Acta* **156**, 261-266 (2015).

122. Michaelson, H. B., The work function of the elements and its periodicity. *J. Appl. Phys.* **48**, 4729-4733 (1977).

123. Rut'kov, E. V., Afanas'eva, E. Y. & Gall, N. R., Graphene and graphite work function depending on layer number on Re. *Diamond Relat. Mater.* **101**, 107576 (2020).

124. Roy-Mayhew, J. D., Bozym, D. J., Punckt, C. & Aksay, I. A., Functionalized graphene as a catalytic counter electrode in dye-sensitized solar cells. *Acs Nano* **4**, 6203-6211 (2010).

125. Matteocci, F., Cinà, L., Di Giacomo, F., Razza, S., Palma, A. L., Guidobaldi, A., D'Epifanio, A., Licoccia, S., Brown, T. M., Reale, A. & Di Carlo, A., High efficiency photovoltaic module based on mesoscopic organometal halide perovskite. *Progress in Photovoltaics: Research and Applications* **24**, 436-445 (2016).

126. Schroder, D. K., Contact resistance and Schottky barriers. *Semiconductor Material and Device Characterization, Third Edition*, 127-184 (2006).

127. Sastrawan, R., Renz, J., Prahl, C., Beier, J., Hinsch, A. & Kern, R., Interconnecting dye solar cells in modules—I–V characteristics under reverse bias. *J. Photochem. Photobiol. A: Chem.* **178**, 33-40 (2006).

128. Lee, W. J., Ramasamy, E., Lee, D. Y. & Song, J. S., Dye-sensitized solar cells: Scale up and current–voltage characterization. *Sol. Energy Mater. Sol. Cells* **91**, 1676-1680 (2007).

129. Bao, W., Wan, J., Han, X., Cai, X., Zhu, H., Kim, D., Ma, D., Xu, Y., Munday, J. N., Drew, H. D., Fuhrer, M. S. & Hu, L., Approaching the limits of transparency and conductivity in graphitic materials through lithium intercalation. *Nature Communications* **5**, 4224 (2014).

130. Saha, S., Hilali, M., Onyegam, E., Sarkar, D., Jawarani, D., Rao, R., Matthew, L., Smith, R., Xu, D., Sopori, B. & Banerjee, S., Single Heterojunction Solar Cells on Exfoliated Flexible ~25..mu.. Thick Mono-Crystalline Silicon Substrates. *Appl. Phys. Lett.* **102**, (2013).

131. Sommeling, P. M., Späth, M., Smit, H. J. P., Bakker, N. J. & Kroon, J. M., Long-term stability testing of dye-sensitized solar cells. *J. Photochem. Photobiol. A: Chem.* **164**, 137-144 (2004).

132. Bari, D., Wrachien, N., Tagliaferro, R., Penna, S., Brown, T. M., Reale, A., Di Carlo, A., Meneghesso, G. & Cester, A., Thermal stress effects on Dye-Sensitized Solar Cells (DSSCs). *Microelectronics Reliability* **51**, 1762-1766 (2011).

133. Di Risio, S. & Yan, N., Piezoelectric Ink-Jet Printing of Horseradish Peroxidase: Effect of Ink Viscosity Modifiers on Activity. *Macromol. Rapid Commun.* **28**, 1934-1940 (2007).

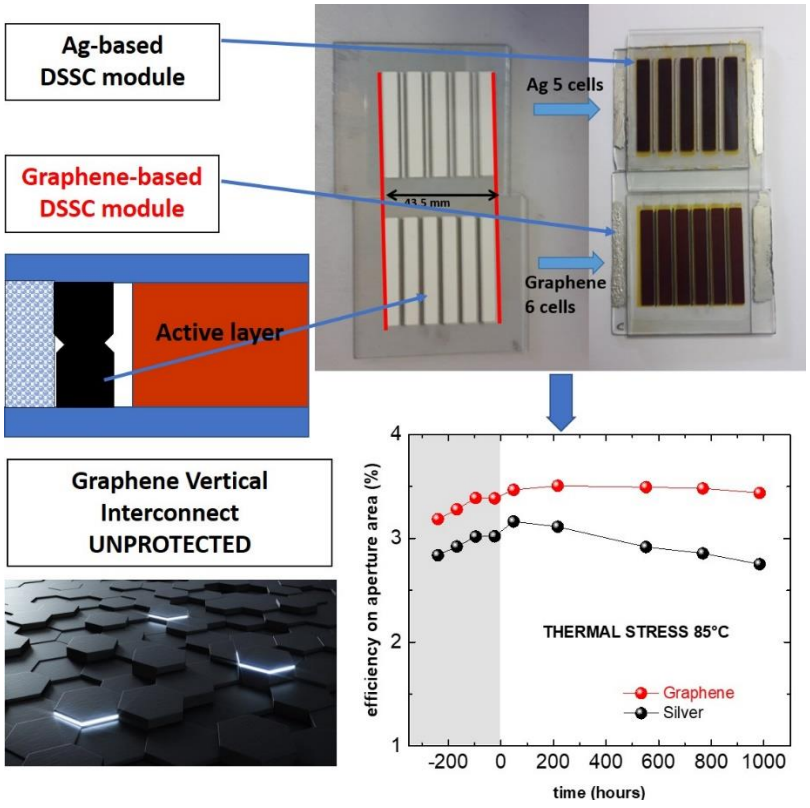

TOC Image: detail of section of graphene-based interconnects (up left) unprotected by sealant. It corresponds to the black line in the photograph (up right). This photography shows that in the case of graphene-based device it is possible to accommodate 6 cells in the same space in which are accommodate 5 cells in the case of silver-base devices, whose interconnects are protected on both sides. This results in a higher APA efficiency of the graphene-based devices and in their higher stability under thermal stress, with respect to silver-based devices as shown in the graph (down right)